AGU PUBLICATIONS

Geophysical Research Letters

RESEARCH LETTER
10.1002/2018GL077032

Key Points:
- Deep convection is sensitive to humidity above the boundary layer; sounding data over tropical oceans are used to study this sensitivity
- We observe warm anomalies, likely strong enough to hinder subsequent convection, above the boundary layer after precipitation
- As the warm anomalies appear only in dry regions, they may offer a new explanation for the sensitivity of deep convection to humidity

Supporting Information:
- Supporting Information S1

Correspondence to:
M. Virman,
meri.virman@helsinki.fi

Citation:
Virman, M., Bister, M., Sinclair, V. A., Järvinen, H., & Räisänen, J. (2018). A new mechanism for the dependence of tropical convection on free-tropospheric humidity. *Geophysical Research Letters*, *45*, 2516–2523. https://doi.org/10.1002/2018GL077032

Received 5 JAN 2018
Accepted 9 FEB 2018
Accepted article online 13 FEB 2018
Published online 10 MAR 2018

A New Mechanism for the Dependence of Tropical Convection on Free-Tropospheric Humidity

M. Virman[1], M. Bister[1], V. A. Sinclair[1], H. Järvinen[1], and J. Räisänen[1]

[1] Institute for Atmospheric and Earth System Research/Physics, Faculty of Science, University of Helsinki, Helsinki, Finland

Abstract Atmospheric deep convection is responsible for transport of the most important greenhouse gas, water vapor, to the free-troposphere and for most of the precipitation on Earth. Observations show that deep convection is strongly sensitive to the amount of moisture in the low-to-midtroposphere. The current understanding is that this sensitivity is due to entrainment. In this study, it is found that over tropical oceans shallow warm anomalies, likely strong enough to hinder subsequent convection, are observed just above the boundary layer after precipitation, but only where the low-to-midtroposphere is dry. The results, showing a cold anomaly above the warm anomaly, suggest that evaporation of stratiform precipitation and subsidence warming below likely cause these temperature anomalies. Evaporation of stratiform precipitation should therefore be a topic of high priority for developing more realistic theories of convective weather phenomena and for improving climate and weather forecast models.

1. Introduction

Atmospheric deep convection is the basic mechanism behind a myriad of important weather phenomena. It is also a major source of water vapor in the free-troposphere. In climate models, the water vapor feedback approximately doubles the warming due to anthropogenic increase of CO_2 (Manabe & Wetherald, 1967). Therefore, understanding the physical processes leading to the development of deep convection is of great importance for both climate predictions and weather forecasts.

Many studies have shown that precipitation is sensitive to column water vapor (Bretherton et al., 2004; Holloway & Neelin, 2009; Neelin et al., 2009; Peters & Neelin, 2006) and low-to-midtropospheric water vapor (Brown & Zhang, 1997; Sherwood, 1999; Sobel et al., 2004), so that a moister low-to-midtroposphere favors convection. Over tropical oceans, the relationship between precipitation and column water vapor is seen in monthly and daily timescales (Bretherton et al., 2004; Holloway & Neelin, 2009; Neelin et al., 2009), whereas over tropical land areas it is strong even on timescales of 15 min to 3 h (Schiro et al., 2016).

Entrainment of environmental air into updrafts can at least partially explain the sensitivity of precipitation to humidity seen in observations (Holloway & Neelin, 2009; Schiro et al., 2016) and in models (Derbyshire et al., 2004; Hirons et al., 2013). Despite extensive attempts, an entrainment rate leading to realistic representation of convection in models has been difficult to find (Mapes & Neale, 2011). Different methods have been applied to make the development of convection sensitive enough to dry air without diluting updrafts too much (Bechtold et al., 2008; Mapes & Neale, 2011; Pan & Randall, 1998; Piriou et al., 2007). For example, Mapes and Neale (2011) made entrainment to depend on parameterized organization of convection, whereas Bechtold et al. (2008) simply made entrainment to be proportional to relative humidity (RH).

It is important to account for a possibility of other yet unknown processes that could cause the sensitivity of convection to low-to-midtropospheric humidity. Here we study sounding and precipitation data and find another potential mechanism related to evaporation of stratiform precipitation. The data and methods are described in section 2. The results are presented in section 3 and discussed in section 4. The conclusions are provided in section 5.

2. Data and Methods

2.1. Data

In this study, the vertical temperature structures associated with precipitation were analyzed using sounding and precipitation data over the eastern Indian Ocean and the western Pacific Ocean. The data were

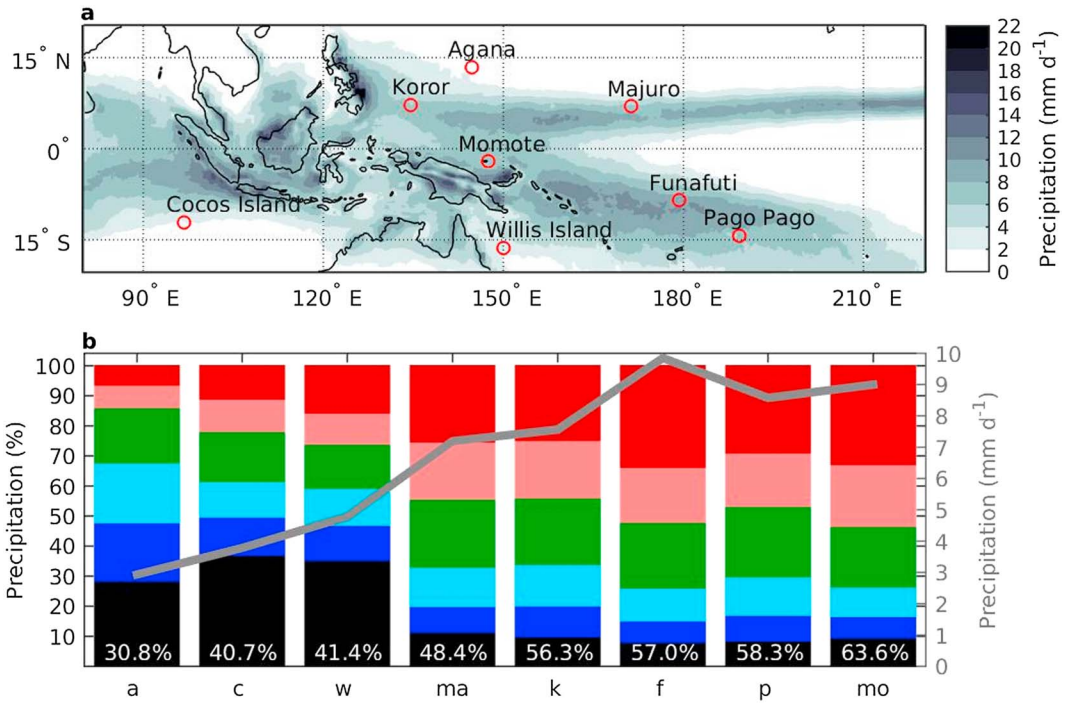

Figure 1. (a) Locations of the sounding stations (red circles) and the mean Tropical Rainfall Measuring Mission precipitation from November to February 1998–2014 (shading) in mm d^{-1}. (b) Percentage of days that fall to PR0 (black), PR1 (dark blue), PR2 (blue), PR3 (green), PR4 (magenta), and PR5 (red) at Agana ("a"), Cocos Is. ("c"), Willis Is. ("w"), Majuro ("ma"), Koror ("k"), Funafuti ("f"), Pago Pago ("p"), and Momote ("mo"). The stations are in order based on the 500–700 hPa climatological mean relative humidity (numbers in white) from the driest (Agana) to the moistest (Momote) station. The gray line shows the mean precipitation over the station in mm d^{-1}.

analyzed over eight sounding stations located in regions with frequent precipitation (Figure 1) during November–February 1998–2014. The soundings were obtained from the Integrated Global Radiosonde Archive version 1 data set. Only soundings that (1) passed the Integrated Global Radiosonde Archive version 1 quality assurance (Durre et al., 2006), (2) have observations of both temperature and dew point depression, (3) have more than one observation in a 200 hPa thick layer and more than six observations in total, and (4) reach the 500 hPa level were included. In Funafuti, unrealistic dew point depression values were occasionally observed and therefore soundings with dew point temperatures colder than −15°C below 900 hPa level (from hereon below means larger pressures) in Funafuti were omitted. Each sounding was interpolated linearly in the vertical to 1 hPa resolution, but no interpolation in time was made. RH and virtual temperature were calculated using the equations in Emanuel (1994). Only one sounding for each day was selected, and the sounding time was 22, 23, 00, or 01 universal time coordinated (UTC).

For precipitation data, the Tropical Rainfall Measuring Mission (TRMM) 3B42 version 7 daily precipitation product (Huffman et al., 2007) was used. This data set has a spatial resolution of 0.25° × 0.25°, and each value represents the accumulated precipitation amount from 22:30 UTC to 22:30 UTC the next day. Therefore, most soundings are from just after the 24 h precipitation period.

The sensitivity of the results (section 3) to variation in local sea surface temperatures (SSTs), the El Niño–Southern Oscillation (ENSO), the occurrence of convectively coupled Kelvin waves (CCKW), and the Madden-Julian Oscillation (MJO) was also studied. For SST and ENSO, the National Oceanic and Atmospheric Administration High-resolution Blended Analysis of Daily SST and Seasonal ERSSTv4 "Oceanic Nino Index" data sets were used. To identify whether a CCKW or MJO occurred, software that applies Fourier filtering to ERA-Interim reanalysis (Dee et al., 2011) outgoing longwave radiation data for the wave numbers and frequencies associated with CCKWs and MJO (Wheeler & Kiladis, 1999) was used. The threshold of ±10 W m^{-2} was used to define a CCKW and MJO (Gottschalck et al., 2013). The ERA-Interim data at 0.75° spatial resolution from 00 UTC was used to study the climatological vertical wind shear. See Text S1 in the supporting information for detailed information.

2.2. Methods

To study the vertical temperature structures associated with precipitation, soundings made after precipitation were compared to soundings made after no precipitation. In the tropical free-troposphere, temperature anomalies associated with precipitating systems propagate over large distances due to the large Rossby radius of deformation. Therefore, the TRMM daily precipitation rates were first averaged over 5° × 5° areas selected so that the station was approximately in the middle of the area. The soundings at each station were divided into six groups based on the amount of daily area-averaged precipitation obtained during the preceding 24 h in the 5° × 5° area. This time interval is representative of a typical duration of a mesoscale convective system (MCS) and also not too different from the boundary layer recovery time (Saxen & Rutledge, 1998; Young et al., 1995).

The area-averaged precipitation thresholds for the six precipitation groups were selected to be <0.5 (PR0), 0.5–1 (PR1), 1–2 (PR2), 2–5 (PR3), 5–10 (PR4), and >10 mm d^{-1} (PR5). The nonprecipitating group (PR0) has a threshold of 0.5 mm d^{-1} instead of 0 mm d^{-1}, because days with zero daily 5° × 5° area-averaged precipitation occur rarely in the TRMM data set.

As temperature changes in the tropics are usually small, it is more convenient to study vertical profiles of temperature anomalies rather than of absolute temperatures. First, for each precipitation group (PR0–PR5) at each station, a mean vertical profile of temperature was calculated. Second, for each station the average of the mean vertical temperature profiles over all six precipitation groups (PR0–PR5) was calculated and this average profile is referred to as the "piecewise mean" profile. Then, to obtain the anomalies with respect to the piecewise mean, the piecewise mean was subtracted from each of the PR0–PR5 group mean temperature profiles.

The piecewise mean vertical profile of temperature (Figures 2a, 2c, and 2e) differs from the climatological mean temperature profile, which would simply be the arithmetic average of soundings from that station. If the climatological mean was subtracted, the resulting temperature anomalies for groups with high precipitation amounts would be larger over dry than moist stations. This is because over the dry stations the climatological mean would be affected more by days with low (PR0–PR1) than high (PR4–PR5) precipitation amounts, whereas over the moist stations the latter (PR4–PR5) dominate. Therefore, subtracting the piecewise mean temperature profile allows comparison of the eight stations representing different RH and precipitation climatologies (Figure 1b), as all of the precipitation groups (PR0–PR5) have the same weight in the piecewise mean. The temperature profile in the nonprecipitating group (PR0) could be subtracted to obtain the temperature anomalies. However, because the PR0 mean temperature profile differs considerably between the stations, this would make comparison of the stations difficult.

3. Results

3.1. Vertical Profiles of Temperature Anomalies

Figures 2 and S1 and S2 show that temperatures in the precipitating groups (PR1–PR5) were generally warmer above 500 hPa, colder between 500 and 700 hPa, warmer between 800 and 950 hPa, and colder below 950 hPa, than in the nonprecipitating group (PR0). For clarity of discussion, we use the term warm (cold) anomaly for temperature anomalies that increase (decrease), in at least quasi-regular manner, from PR0 to PR5. Even though, for example, in Agana in the 800–950 hPa layer the temperature anomalies in PR1–PR3 groups were negative relative to the piecewise mean, temperatures in all of the precipitating groups (PR1–PR5) were still warmer than in the nonprecipitating group (PR0, Figures 2a and 2b). The warm anomalies above 500 hPa and the cold anomalies below 950 hPa were observed at most precipitating groups (PR1–PR5) at most stations, whereas a clear 500–700 hPa cold anomaly was observed at all stations except Momote (Figures 2 and S1 and S2). These temperature anomalies correspond to diabatic heating structures in MCSs: latent heating in the anvils of MCSs above 500 hPa, cooling immediately below the anvil base at 500 hPa associated with evaporation and melting of stratiform precipitation, and near-surface cooling due to convective-scale downdrafts (Houze, 1982).

The temperature anomaly profiles reveal a shallow warm anomaly between 800 and 950 hPa (Figures 2a–2d and S1a–S1e) occurring after precipitation. The magnitude of this warm anomaly is related to the climatological mean RH of the station in the 500–700 hPa layer (Figure 3a). Over the driest stations, a warm anomaly that is larger with higher amounts of previous precipitation is observed, but over the most moist stations no warm anomaly is observed even after intense precipitation (Figures 2e and 2f and S1f–S1h). Also, over

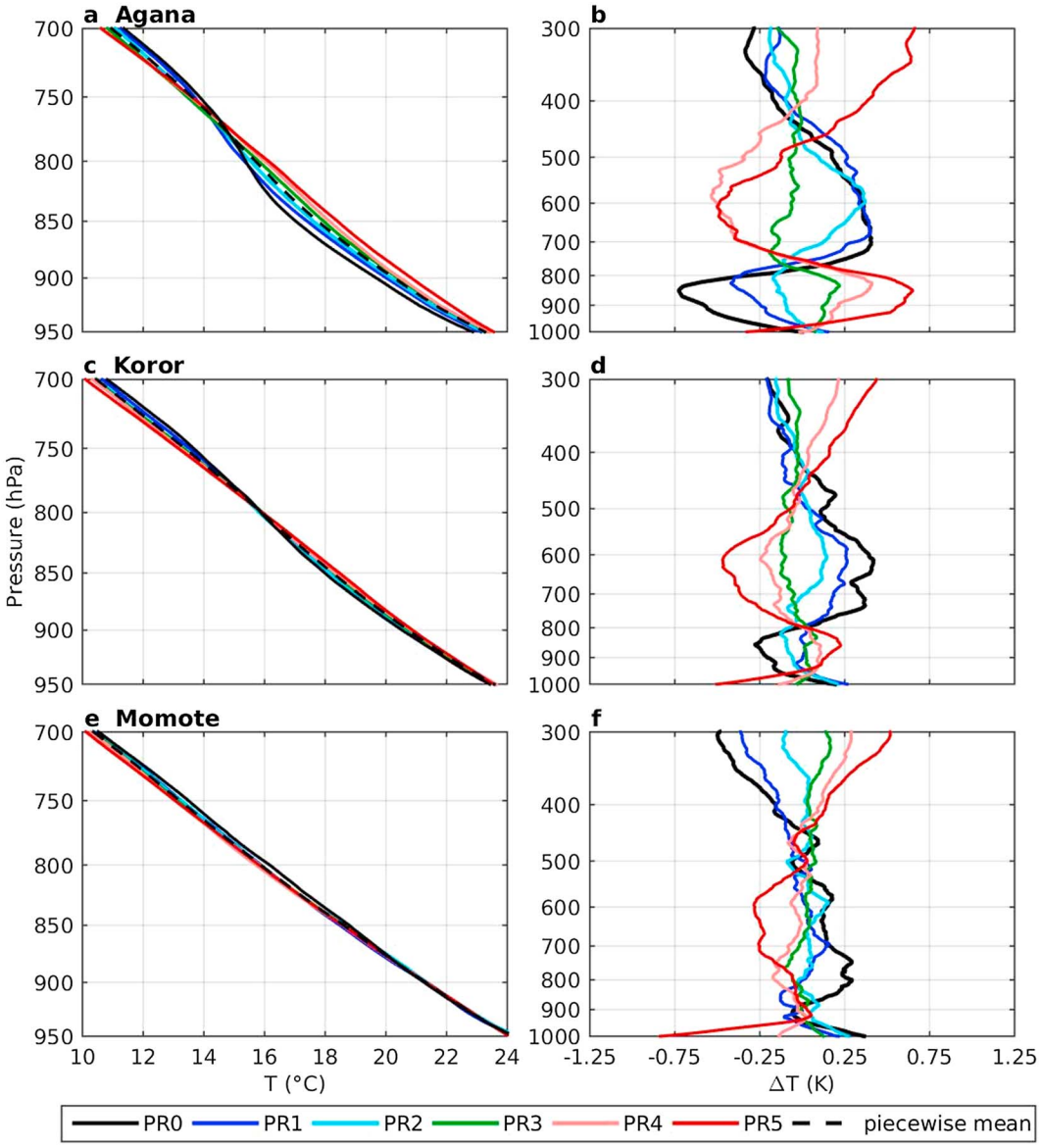

Figure 2. Vertical profiles of absolute temperature (*T*) and temperature anomaly with respect to the piecewise mean (ΔT) in Agana (a and b), Koror (c and d), and Momote (e and f). Note the different vertical scales between the left and right columns.

the most moist stations water vapor mixing ratio varies less with precipitation (Figures S3f–S3h) than over the driest stations (Figures S3a–S3e). The effect of the warm anomaly on subsequent convection is discussed in section 3.2. The magnitude of the cold anomaly between roughly 500 and 700 hPa has a weak dependence on the 500–700 hPa climatological mean RH (Figure 3b), most likely because the cold anomaly may have been partly produced by the melting of ice, a process which only weakly depends on RH.

The formation mechanism of the 800–950 hPa warm anomaly is most likely associated with evaporation in the roughly 500–700 hPa layer and induced subsidence below. We conclude this because (1) the warm anomaly occurs below the 500–700 hPa cold anomaly (Figures 2b, 2d, and S1a–S1e) and (2) its occurrence and magnitude are related to the 500–700 hPa climatological mean RH and precipitation amount (Figure 3a). No warm anomaly is observed in the most moist stations, and this is hypothesized to be due to, first, weaker subsidence resulting from weaker evaporation above the 800–950 hPa layer and, second, more precipitation reaching the 800–950 hPa layer and evaporating there. The mechanism is further discussed in section 4. Large climatological 800–1000 hPa vertical wind shear (Figure S4) suggests that the environment over Cocos Island is favorable

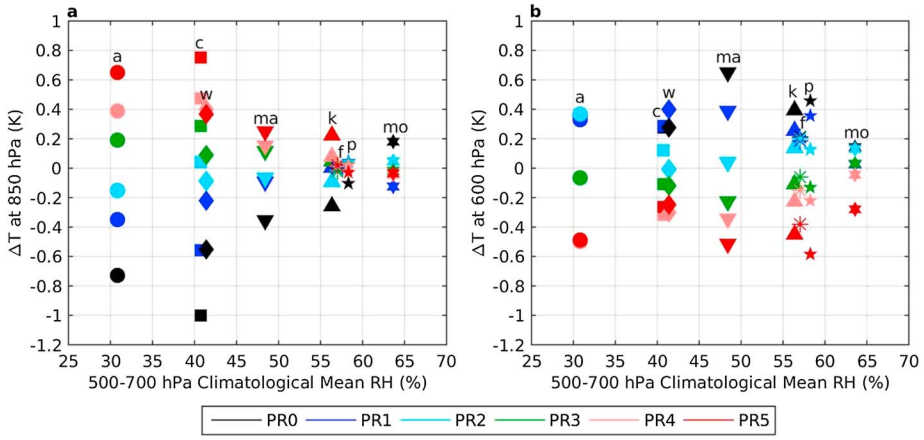

Figure 3. The (a) 850 hPa and (b) 600 hPa temperature anomaly with respect to the piecewise mean (ΔT) in the precipitation groups and at different stations (see Figure 1 caption for letters) as function of the 500–700 hPa climatological mean relative humidity (RH).

for squall lines. In squall lines, evaporation of precipitation is enhanced as dry air from the environment enters the precipitating system, which may explain why the warm anomaly in Cocos Island is an outlier in Figure 3a.

The temperature in the lower troposphere is affected by several other meteorological phenomena, such as variation in local SST, ENSO, the occurrence of CCKWs (Herman et al., 2016; Kiladis et al., 2009), and the MJO. To eliminate these as causes of the 800–950 hPa warm anomaly, the analysis was repeated but for smaller subgroups of the data which have less variability in the above mentioned phenomena (see Text S1). The relation between the 800–950 hPa warm anomaly and the 500–700 hPa climatological mean RH is still observed in all of the new subgroups (Figures S5–S9). This strongly suggests that the warm anomaly is not produced by the above mentioned phenomena.

3.2. Effect of the Warm Anomaly on Buoyancy

The temperature, or more precisely virtual temperature, difference between a rising air parcel and the environment determines whether convection is possible. Therefore, the warm anomalies just above the boundary layer may explain why subsequent deep convection depends on low-to-midtropospheric humidity. The effect of the 800–950 hPa warm anomaly on the environmental virtual temperature profile was quantified by subtracting the mean virtual temperature profile in the nonprecipitating group (PR0) from the mean virtual temperature profile in the group with highest precipitation amounts (PR5). In Agana, which is the driest station, this virtual temperature difference was 1.3 K at 850 hPa and in Koror the virtual temperature difference is still as much as 0.5 K, whereas over the moistest station, Momote, no clear warm anomaly is observed (Figure 4). Over the West Pacific, observations have shown that virtual temperature differences between cloud updrafts and environmental air are only about 0.5 K at 850 hPa (Wei et al., 1998). Therefore, the 800–950 hPa warm anomalies we observe over the dry stations (Figure 4) are probably large enough to reduce the buoyancy so much as to provide a hostile environment for future deep convection. The relatively large time and spatial scales used in this study imply that the warm anomalies likely persist long enough to affect future deep convection.

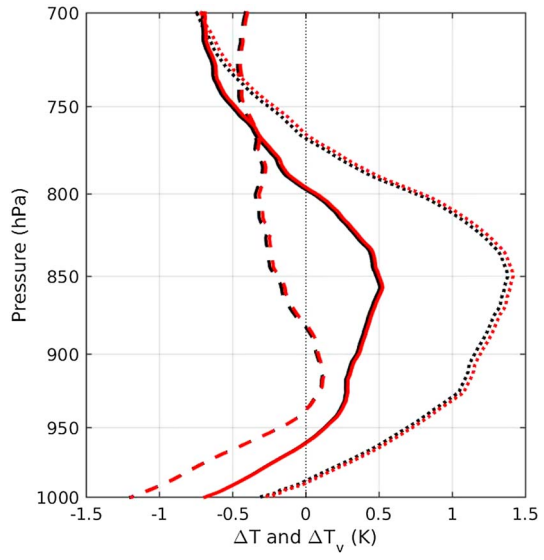

Figure 4. The vertical profile of the temperature (ΔT, black) and virtual temperature (ΔT_v, red) difference between the PR5 and PR0 groups (PR5 minus PR0) in Agana (dotted), Koror (solid), and Momote (dashed).

4. Discussion

In this study, the data set contains the whole spectrum of precipitating tropical cloud systems. The results suggest that warm anomalies just above the boundary layer are a ubiquitous feature associated with deep tropical convection from Indian Ocean to the western Pacific Ocean. Interestingly, Zehr (1976), in a study comparing pretyphoon cloud clusters to

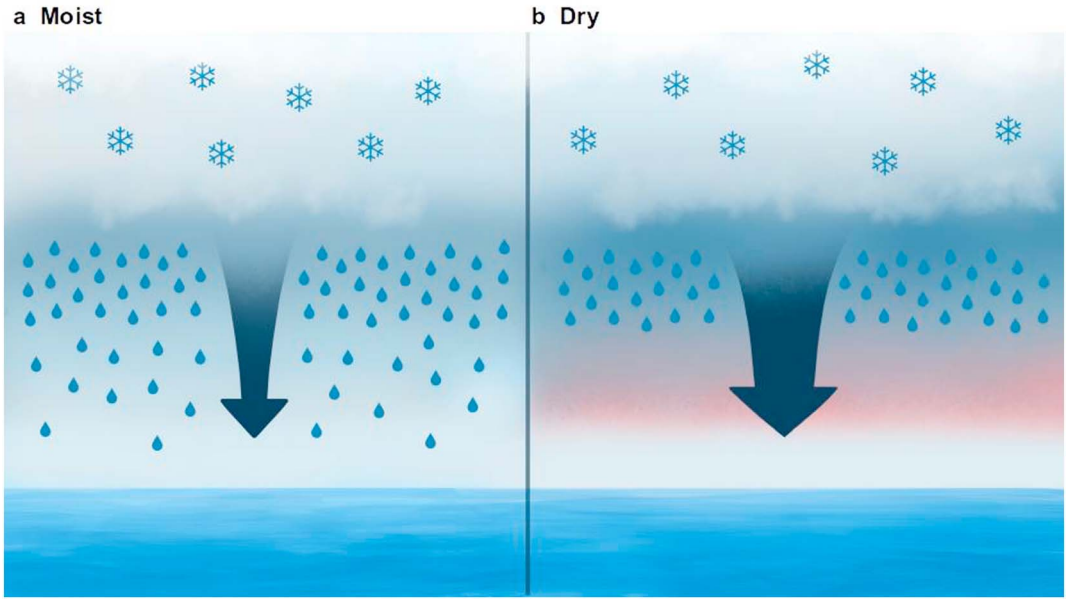

Figure 5. Illustration of the hypothesized mechanism causing the observed cold (blue) and warm (red) anomalies below an upper tropospheric precipitating anvil at moist (a) and dry (b) stations. The arrows denote the subsidence due to evaporation, with the width of the arrow corresponding to the relative strength of the subsidence.

nondeveloping cloud clusters over western Pacific Ocean, found in nondeveloping clusters a warm anomaly just above the boundary layer that closely resembles the anomaly seen in our results.

Previously, warm anomalies just above the boundary layer have been observed in the trailing parts of propagating squall lines (Zipser, 1977), which have been hypothesized to be due to evaporative mesoscale downdrafts (Zipser, 1969, 1977) and the downward overshooting of such downdrafts (Zipser, 1977, and references therein). Miller and Betts (1977) suggested that the mesoscale downdraft is dynamically driven and associated with descent over a spreading cold outflow fed by convective-scale downdrafts.

The 800–950 hPa warm anomaly does not seem to be due to a dynamically driven downdraft above a spreading cold outflow because the cold anomaly in the boundary layer is actually coldest over the moist stations which do not have the warm anomaly. Because the warm anomalies are found under a 500–700 hPa cold anomaly (Figure 2) suggests that they are associated with evaporative cooling of stratiform precipitation. In a process simulation with an axisymmetric model, Bister and Emanuel (1997) found a warm anomaly to develop beneath a cold anomaly as a result of subsidence induced by evaporation of stratiform rain.

In Figure 5, the hypothesized formation mechanism of the 800–950 hPa warm anomaly is shown. In a moist atmosphere, rain from an anvil cloud evaporates in the whole lower troposphere resulting in a cold anomaly there. In a dry atmosphere, evaporation is enhanced just below the base of the anvil cloud. The enhanced evaporation just below the anvil base leads to, first, the subsidence being stronger, even below evaporation, due to effects of hydrostatic pressure changes. Second, this enhanced evaporation leads to little rain available for evaporation lower down. Therefore, a warm anomaly can form below the cold anomaly.

The appearance of the 800–950 hPa warm anomaly can also be explained using gravity wave dynamics. Mapes (1993) showed how gravity wave dynamics cause the diabatic heating profile of an MCS to lead to temperature anomalies close to the MCS. That study showed that a positive-only diabatic heating profile typical of that observed in MCSs over the world's warmest waters (where the troposphere is relatively moist and corresponding to the locations of our moist stations) leads to a cold anomaly in the whole lower troposphere close to the MCS, and this could favor the formation of self-organizing superclusters (Mapes & Houze, 1993). Our study shows that over the drier stations, a warm anomaly, instead of a cold anomaly, is observed just above the boundary layer after precipitation. We suggest that different vertical structure of evaporation of stratiform precipitation in dry and moist air is the ultimate reason for the different temperature anomalies in MCSs forming in dry and moist areas, respectively.

This study has some limitations. First of all, the analysis is restricted to relatively large time and spatial scales because in the tropics temperature anomalies associated with nonlocal precipitation should also be accounted for. Second, for evaporation, the optimal measure of humidity would be instantaneous local humidity, not climatological humidity. However, instantaneous values are affected by both previous and remote precipitation, which also lead to temperature anomalies. Therefore, studying causal relationships with an observational data set and instantaneous humidities is not a simple task. Fine-scale modeling studies will be conducted to better understand the suggested mechanism as then humidity can be used as an independent initial condition.

5. Conclusions

In this study, sounding and precipitation data were analyzed over the eastern Indian Ocean and western Pacific Ocean to study the vertical temperature profiles associated with precipitation from the preceding 24 h. Warm anomalies between 800 and 950 hPa were observed after precipitation, but only over stations with low climatological 500–700 hPa mean RH. Over dry stations, these warm anomalies were larger with higher amounts of previous precipitation, but over the moist stations the warm anomalies did not develop even after intense precipitation. That the warm anomalies occurred below a cold anomaly between 500 and 700 hPa and only over the dry stations suggests that the warm anomalies developed due to subsidence warming below a layer of evaporation of stratiform precipitation. The 800–950 hPa warm anomalies are likely large enough to diminish the possibility of new convection as long as the warm anomaly lasts.

Accounting for this suggested mechanism of convection's sensitivity to low-to-midtropospheric moisture has potential to pave the way to more comprehensive theories for convective phenomena, for example, MJO (Zhang, 2005). Stratiform precipitation and especially its evaporation need to be accurately represented in numerical weather prediction and climate models to allow this mechanism to occur in them. Specifically, a prerequisite for realistic climate projections is that the climate models predict the amount of water vapor in the free-troposphere correctly. This requires that convection (a major source of water vapor in the free-troposphere) in the models occurs due to right physical reasons, that is, the mechanisms of convection's sensitivity to humidity are right, and also that the vertical velocities in convection are correct (Parodi & Emanuel, 2009). A realistic representation of the new mechanism is expected to be important to reach these goals.

Acknowledgments

We thank P. Bechtold, H. Savijärvi, V.-M. Kerminen, and two anonymous reviewers for their helpful suggestions on the manuscript and S. Lindström for producing Figure 5. All data sets used are public, and codes are available from M. V. upon request. The TRMM 3B42 daily data were provided by the NASA/GSFC/MMPL/PPS at the NASA/GES DISC Mirador portal (https://disc.gsfc.nasa.gov/datacollection/TRMM_3B42_Daily_7.html), the IGRA soundings by the NOAA NCEI (https://www.ncdc.noaa.gov/data-access/weather-balloon/integrated-global-radiosonde-archive), the ONI data set by NWS/CPC/OAD library (http://www.cpc.ncep.noaa.gov/data/indices/), the SST data by the NOAA/OAR/ESRL PSD (https://www.esrl.noaa.gov/psd/data/gridded/data.noaa.oisst.v2.highres.html), and the ERA-Interim OLR data by the ECMWF from MARS. The CCKW/MJO software was developed by M. Herman and adapted for ECMWF by P. Bechtold. M. V. is funded by the Vilho, Yrjö, and Kalle Väisälä Foundation, and V. A. S. is funded by the Academy of Finland (project 3073314). M. V. was also supported by the Tiina and Antti Herlin Foundation.

References

Bechtold, P., Köhler, M., Jung, T., Doblas-Reyes, F., Leutbecher, M., Rodwell, M. J., et al. (2008). Advances in simulating atmospheric variability with the ECMWF model: From synoptic to decadal time-scales. *Quarterly Journal of the Royal Meteorological Society*, *134*(634), 1337–1351. https://doi.org/10.1002/qj.289

Bister, M., & Emanuel, K. A. (1997). The genesis of Hurricane Guillermo: TEXMEX analyses and a modeling study. *Monthly Weather Review*, *125*(10), 2662–2682. https://doi.org/10.1175/1520-0493(1997)125<2662:TGOHGT>2.0.CO;2

Bretherton, C. S., Peters, M. E., & Back, L. E. (2004). Relationships between water vapor path and precipitation over the tropical oceans. *Journal of Climate*, *17*(7), 1517–1528. https://doi.org/10.1175/1520-0442(2004)017<1517:RBWVPA>2.0.CO;2

Brown, R. G., & Zhang, C. (1997). Variability of midtropospheric moisture and its effect on cloud-top height distribution during TOGA COARE. *Journal of the Atmospheric Sciences*, *54*(23), 2760–2774. https://doi.org/10.1175/1520-0469(1997)054<2760:VOMMAI>2.0.CO;2

Dee, D., Uppala, S., Simmons, A., Berrisford, P., Poli, P., Kobayashi, S., et al. (2011). The ERA-Interim Reanalysis: Configuration and performance of the data assimilation system. *Quarterly Journal of the Royal Meteorological Society*, *137*(656), 553–597. https://doi.org/10.1002/qj.828

Derbyshire, S., Beau, I., Bechtold, P., Grandpeix, J., Piriou, J., Redelsperger, J., & Soares, P. (2004). Sensitivity of moist convection to environmental humidity. *Quarterly Journal of the Royal Meteorological Society*, *130*(604), 3055–3079. https://doi.org/10.1256/qj.03.130

Durre, I., Vose, R. S., & Wuertz, D. B. (2006). Overview of the Integrated Global Radiosonde Archive. *Journal of Climate*, *19*(1), 53–68. https://doi.org/10.1175/JCLI3594.1

Emanuel, K. A. (1994). *Atmospheric convection*. New York: Oxford University Press.

Gottschalck, J., Roundy, P. E., Schreck III, C. J., Vintzileos, A., & Zhang, C. (2013). Large-scale atmospheric and oceanic conditions during the 2011–12 DYNAMO field campaign. *Monthly Weather Review*, *141*(12), 4173–4196. https://doi.org/10.1175/MWR-D-13-00022.1

Herman, M. J., Fuchs, Z., Raymond, D. J., & Bechtold, P. (2016). Convectively coupled Kelvin waves: From linear theory to global models. *Journal of the Atmospheric Sciences*, *73*(1), 407–428. https://doi.org/10.1175/JAS-D-15-0153.1

Hirons, L., Inness, P., Vitart, F., & Bechtold, P. (2013). Understanding advances in the simulation of intraseasonal variability in the ECMWF model. Part II: The application of process-based diagnostics. *Quarterly Journal of the Royal Meteorological Society*, *139*(675), 1427–1444. https://doi.org/10.1002/qj.2059

Holloway, C. E., & Neelin, J. D. (2009). Moisture vertical structure, column water vapor, and tropical deep convection. *Journal of the Atmospheric Sciences*, *66*(6), 1665–1683. https://doi.org/10.1175/2008JAS2806.1

Houze, R. A. (1982). Cloud clusters and large-scale vertical motions in the tropics. *Journal of the Meteorological Society of Japan. Series II*, *60*(1), 396–410. https://doi.org/10.2151/jmsj1965.60.1_396

Huffman, G. J., Bolvin, D. T., Nelkin, E. J., Wolff, D. B., Adler, R. F., Gu, G., et al. (2007). The TRMM Multisatellite Precipitation Analysis (TMPA): Quasi-global, multiyear, combined-sensor precipitation estimates at fine scales. *Journal of Hydrometeorology*, *8*(1), 38–55. https://doi.org/10.1175/JHM560.1

Kiladis, G. N., Wheeler, M. C., Haertel, P. T., Straub, K. H., & Roundy, P. E. (2009). Convectively coupled equatorial waves. *Reviews of Geophysics*, *47*, RG2003. https://doi.org/10.1029/2008RG000266

Manabe, S., & Wetherald, R. T. (1967). Thermal equilibrium of the atmosphere with a given distribution of relative humidity. *Journal of the Atmospheric Sciences*, *24*(3), 241–259. https://doi.org/10.1175/1520-0469(1967)024<0241:TEOTAW>2.0.CO;2

Mapes, B., & Neale, R. (2011). Parameterizing convective organization to escape the entrainment dilemma. *Journal of Advances in Modeling Earth Systems*, *3*, M06004. https://doi.org/10.1029/2011MS000042

Mapes, B. E. (1993). Gregarious tropical convection. *Journal of the Atmospheric Sciences*, *50*(13), 2026–2037. https://doi.org/10.1175/1520-0469(1993)050<2026:GTC>2.0.CO;2

Mapes, B. E., & Houze, R. A. (1993). Cloud clusters and superclusters over the oceanic warm pool. *Monthly Weather Review*, *121*(5), 1398–1416. https://doi.org/10.1175/1520-0493(1993)121<1398:CCASOT>2.0.CO;2

Miller, M. J., & Betts, A. K. (1977). Traveling convective storms over Venezuela. *Monthly Weather Review*, *105*(7), 833–848. https://doi.org/10.1175/1520-0493(1977)105<0833:TCSOV>2.0.CO;2

Neelin, J. D., Peters, O., & Hales, K. (2009). The transition to strong convection. *Journal of the Atmospheric Sciences*, *66*(8), 2367–2384. https://doi.org/10.1175/2009JAS2962.1

Pan, D.-M., & Randall, D. D. A. (1998). A cumulus parametrization with a prognostic closure. *Quarterly Journal of the Royal Meteorological Society*, *124*(547), 949–981. https://doi.org/10.1002/qj.49712454714

Parodi, A., & Emanuel, K. (2009). A theory for buoyancy and velocity scales in deep moist convection. *Journal of the Atmospheric Sciences*, *66*(11), 3449–3463. https://doi.org/10.1175/2009JAS3103.1

Peters, O., & Neelin, J. D. (2006). Critical phenomena in atmospheric precipitation. *Nature physics*, *2*(6), 393–396. https://doi.org/10.1038/nphys314

Piriou, J., Redelsperger, J., Geleyn, J., Lafore, J., & Guichard, F. (2007). An approach for convective parameterization with memory: Separating microphysics and transport in grid-scale equations. *Journal of the Atmospheric Sciences*, *64*(11), 4127–4139. https://doi.org/10.1175/2007JAS2144.1

Saxen, T. R., & Rutledge, S. A. (1998). Surface fluxes and boundary layer recovery in TOGA COARE: Sensitivity to convective organization. *Journal of the Atmospheric Sciences*, *55*(17), 2763–2781. https://doi.org/10.1175/1520-0469(1998)055<2763:SFABLR>2.0.CO;2

Schiro, K. A., Neelin, J. D., Adams, D. K., & Lintner, B. R. (2016). Deep convection and column water vapor over tropical land versus tropical ocean: A comparison between the Amazon and the tropical western Pacific. *Journal of the Atmospheric Sciences*, *73*(10), 4043–4063. https://doi.org/10.1175/JAS-D-16-0119.1

Sherwood, S. C. (1999). Convective precursors and predictability in the tropical western Pacific. *Monthly Weather Review*, *127*(12), 2977–2991. https://doi.org/10.1175/1520-0493(1999)127<2977:CPAPIT>2.0.CO;2

Sobel, A. H., Yuter, S. E., Bretherton, C. S., & Kiladis, G. N. (2004). Large-scale meteorology and deep convection during TRMM KWAJEX*. *Monthly Weather Review*, *132*(2), 422–444. https://doi.org/10.1175/1520-0493(2004)132<0422:LMADCD>2.0.CO;2

Wei, D., Blyth, A. M., & Raymond, D. J. (1998). Buoyancy of convective clouds in TOGA COARE. *Journal of the Atmospheric Sciences*, *55*(22), 3381–3391. https://doi.org/10.1175/1520-0469(1998)055<3381:BOCCIT>2.0.CO;2

Wheeler, M., & Kiladis, G. N. (1999). Convectively coupled equatorial waves: Analysis of clouds and temperature in the wavenumber-frequency domain. *Journal of the Atmospheric Sciences*, *56*(3), 374–399. https://doi.org/10.1175/1520-0469(1999)056<0374:CCEWAO>2.0.CO;2

Young, G. S., Perugini, S. M., & Fairall, C. W. (1995). Convective wakes in the equatorial western Pacific during TOGA. *Monthly Weather Review*, *123*(1), 110–123. https://doi.org/10.1175/1520-0493(1995)123<0110:CWITEW>2.0.CO;2

Zehr, R. (1976). Tropical disturbance intensification, Department of Atmospheric Science Paper, no. 259, Colorado State University Ft, Collins, CO.

Zhang, C. (2005). Madden-Julian Oscillation. *Reviews of Geophysics*, *43*, RG2003. https://doi.org/10.1029/2004RG000158

Zipser, E. J. (1969). The role of organized unsaturated convective downdrafts in the structure and rapid decay of an equatorial disturbance. *Journal of Applied Meteorology*, *8*(5), 799–814. https://doi.org/10.1175/1520-0450(1969)008<0799:TROOUC>2.0.CO;2

Zipser, E. J. (1977). Mesoscale and convective-scale downdrafts as distinct components of squall-line structure. *Monthly Weather Review*, *105*(12), 1568–1589. https://doi.org/10.1175/1520-0493(1977)105<1568:MACDAD>2.0.CO;2